REPORT

MATERIALS SCIENCE

Direction-specific van der Waals attraction between rutile TiO_2 nanocrystals

Xin Zhang,[1]* Yang He,[2]* Maria L. Sushko,[1]* Jia Liu,[3] Langli Luo,[3] James J. De Yoreo,[1] Scott X. Mao,[2]† Chongmin Wang,[3]† Kevin M. Rosso[1]†

Mutual lattice orientations dictate the types and magnitudes of forces between crystalline particles. When lattice polarizability is anisotropic, the van der Waals dispersion attraction can, in principle, contribute to this direction dependence. We report measurement of this attraction between rutile nanocrystals, as a function of their mutual orientation and surface hydration extent. At tens of nanometers of separation, the attraction is weak and shows no dependence on azimuthal alignment or surface hydration. At separations of approximately one hydration layer, the attraction is strongly dependent on azimuthal alignment and systematically decreases as intervening water density increases. Measured forces closely agree with predictions from Lifshitz theory and show that dispersion forces can generate a torque between particles interacting in solution and between grains in materials.

Interfacial forces between crystals that depend on their mutual crystallographic alignment enable diverse multiscale phenomena such as crystal growth by oriented attachment (*1*, *2*), Schiller layer formation (*3*), clay swelling (*4*), adhesion and friction anisotropy (*5*, *6*), and grain boundary structuring in polycrystals (*7*). While the attraction or repulsion of two crystallites is based on a set of forces that are generally well understood (*5*), aspects of these forces that are sensitive to lattice alignment have been more difficult to probe. For example, in oriented attachment, where crystal growth entails self-assembly from nanocrystals, the existence of torque-generating forces that align approaching particles to enable adhesion have been implied more often than proven (*1*, *2*, *8*). For instance, in situ liquid-cell transmission electron microscopy (TEM) measurements showed that particle rotation accelerated when the nanocrystals were nearly coaligned, while still separated by a nanometer of solution (*9*, *10*).

Conceptually, the types of interfacial forces that can be sensitive to relative orientation include Coulombic (due to the structured arrangement of charges at specific interfaces) (*11*), van der Waals (vdW) (for lattices with anisotropic polarizability), solvation (due to the response of solvent to specific surface structure), and ion correlation forces (dispersion-based attraction of ions within interacting surface-specific electrical double layers) (*5*, *12*, *13*). The theoretical underpinnings of these anisotropic forces are well established (*5*), but techniques that can isolate and measure their magnitudes for a given pair of interacting oriented crystal faces have generally been limited to use of macroscopic yet atomically flat single crystals (e.g., mica) (*4*). Lattice-specific adhesion anisotropy between faces of microscopic crystals has been demonstrated (*4*, *14*), but a detailed interpretation of such data is difficult owing to the complex interplay of electrostatic, hydration, and vdW interactions giving rise to the observed total force.

We demonstrate direction-specific vdW dispersion attraction between two rutile TiO_2 (001) nanocrystals (*15*), assessing the role of intervening water systematically and making quantitative comparison to predictions from Lifshitz theory. Critical to these measurements is precise control of surface expression and roughness, interfacial contact area, separation distance, and mutual crystallographic alignment. Atomic force microscopy (AFM)–based force measurements have been useful to some extent—for example, using a (roughly spherical and nonoriented) colloidal probe method (*16*)—but this approach suffers from uncertainties because the interparticle gap is not visualized. To measure force-distance relationships while directly imaging the interparticle gap, we integrated AFM probe technology with environmental TEM (ETEM) (*17*). In the ETEM-AFM approach, the separation distance is measured with high precision in real time. Force-distance relationships are evaluated with a cantilever of known spring constant, computing the force via Hooke's law. This also enables detailed characterization of coplanarity, azimuthal orientation, contact area, and surface roughness throughout force measurements.

The rutile (001) surface was selected because it is dielectrically anisotropic in all three crystallographic directions, including substantial anisotropy in the *a* plane (*18*–*20*) such that the strength of the dispersion interaction should depend on azimuthal alignment along [001]. Also, the rutile (001) surface is readily hydroxylated in air (*21*) and remains so in vacuum at room temperature, thereby avoiding a hydroxylation threshold during water vapor dosing (*22*) and minimizing the chance of chemical reaction of the surfaces upon contact (*15*, *23*).

Atomically flat rutile AFM tips and opposing rutile substrates were fabricated by focused ion beam milling to excise nanocrystals from the surface of a single monolith that was preoriented, cut, and polished to prepare the (001) face (fig. S1) (*15*). The resulting (001) AFM tip (Fig. 1, A to C) and opposing (001) substrate (Fig. 1D) were atomically flat and clean, and their azimuthal orientation across the full symmetrically equivalent range of 0° to 90° was accurately controlled in the TEM by means of diffraction pattern analysis (*15*). Coplanarity of the contact between these nanocrystals was always confirmed to be perfectly face-to-face during measurements (Fig. 1, E and F).

In ETEM-AFM force curve measurements, the rutile (001) substrate is driven toward the rutile (001) nanocrystal on the AFM tip, paused at an applied contact force, and then retracted to its original position, using constant approach and retraction velocity (movies S1 to S3). Figure 2 illustrates a typical force-distance curve for an approach and retraction cycle, with corresponding TEM images. Point 1 denotes the beginning of approach from long range, during which the cantilever remains undeflected (Fig. 2A). When the gradient of the attractive rutile (001)–rutile (001) force exceeds the cantilever stiffness, the nanocrystal tip jumps-to-contact the substrate (point 2, Fig. 2B), and the jump distance is precisely measured. The substrate is further pushed toward the cantilever until the applied force reaches ~20 nN (point 3, Fig. 2C) with a dwell time of ~30 s before beginning retraction. During retraction, the tip remains attractively bound in contact with the substrate (points 4 and 5, Fig. 2, D and E) until the elastic force of the cantilever exceeds the attractive force, at which point the tip jumps-from-contact (point 6, Fig. 2F) and the deflection returns to its rest position over a precisely measured jump distance.

All experiments were performed in controlled water-exposure conditions that ranged from that intrinsic to the high-vacuum background pressure of 10^{-7} mbar up to 10^{-1} mbar of added water vapor (*15*). The initial (001) termination in high vacuum was assumed to be that first stabilized by hydration and hydroxylation during preparation in air, likely involving reconstruction (*24*). Such a situation is ideal because it minimizes the chance that the nanocrystal surfaces react chemically upon water dosing or contact (*22*, *23*). With increasing water background pressure, a molecularly thin hydrated layer of associatively

[1]Physical and Computational Sciences Directorate, Pacific Northwest National Laboratory, Richland, WA, USA. [2]Department of Mechanical Engineering and Materials Science, University of Pittsburgh, Pittsburgh, PA, USA. [3]Environmental Molecular Sciences Laboratory, Pacific Northwest National Laboratory, Richland, WA, USA.
*These authors contributed equally to this work. †Corresponding author. Email: kevin.rosso@pnnl.gov (K.M.R.); chongmin.wang@pnnl.gov (C.W.); sxm2@pitt.edu (S.X.M.)

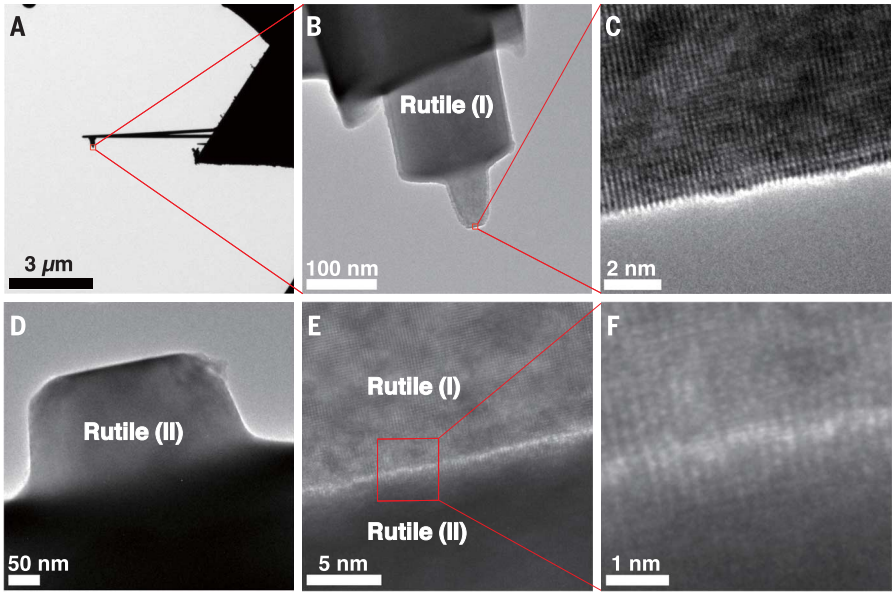

Fig. 1. Characterization of a representative rutile (001) AFM tip and rutile (001) substrate in the ETEM. Low-magnification images of the (**A**) AFM cantilever and (**B**) mounted rutile (001) nanocrystal tip. (**C**) High-resolution image of the nanocrystal tip surface. (**D**) Low-magnification image of the rutile (001) nanocrystal substrate mounted on a gold needle. (**E** and **F**) Low- (E) and high- (F) magnification image of the tip and substrate interface after jump-to-contact at zero applied force, showing face-to-face coplanarity.

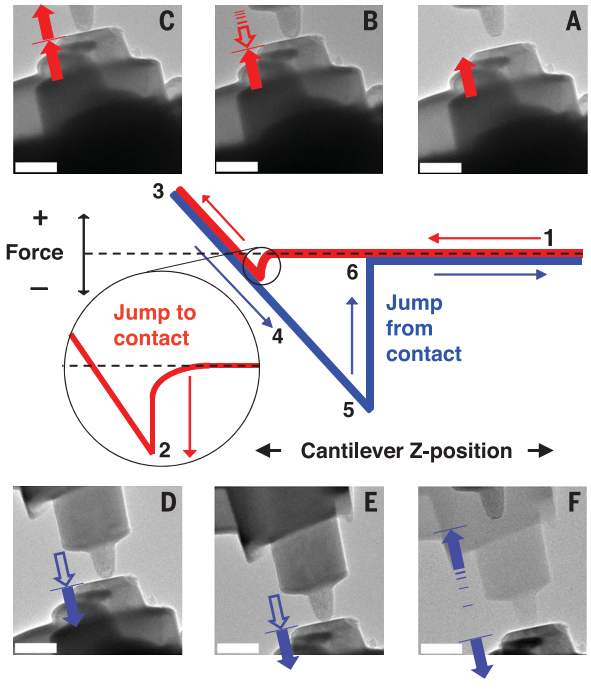

Fig. 2. ETEM-AFM force-distance sequence with corresponding TEM images. Red color denotes the approach sequence, blue denotes retraction. Arrows indicate motion; unfilled arrows denote attractive contact of the tip to substrate under tensile force from the cantilever. (**A**) Two rutile (001) nanocrystals seperated at long range with the substrate approaching the tip. (**B**) Jump-to-contact. (**C**) End of the contact ramp and dwell point at an applied force of 20 nN, after which retraction (**D**) proceeds until (**E**) the deflection limit and (**F**) jump-from-contact returns the cantilever to its initial value. Scale bars, 200 nm.

adsorbed water is expected to grow in density on the hydroxylated terminations until reaching complete coverage at ~10^{-1} mbar (*15*, *21*, *25*, *26*).

Figure 3A shows long-range jump-to-contact forces at different azimuthal orientations (from 0° to 45°) between two rutile (001) nanocrystals, over which the lattice alignment is expected to progress from perfect to maximally misaligned, respectively. The determined attractive force shows no dependence on the azimuthal orientation within the measurement error. Furthermore, the jump-to-contact force in each azimuthal orientation was found to be insensitive to the water vapor pressure in the TEM system, across the full range of pressures explored, indicating no dependence on the water layer adsorbed on the respective (001) surfaces.

Figure 3B shows the short-range jump-from-contact forces at different azimuthal orientations (from 0° to 90°) through the maximally misaligned value (45°) and over the same range of water vapor pressures. In contrast to the long-range forces, in all cases the jump-from-contact force is systematically correlated to the extent of the azimuthal alignment of the two nanocrystals, displaying the expected 90° of rotational symmetry along [001] (Fig. 3C). At each water pressure, the force decreases as the azimuthal orientation is stepped out of alignment from 0° to 45°, then increases at an equivalent inverse rate as alignment is progressively reacquired from 45° to 90°. Thus, at short range, the interparticle attractive forces are direction specific, exhibiting an angular period consistent with the rutile structure and a maximum when the azimuthal orientation is in lattice-matching configurations at around 0° and 90°. Furthermore, the effect of increasing the water pressure, and the coverage of the intervening water layer, is to diminish the adhesive force between the nanocrystals interacting at short range but not the dependence on lattice coalignment. Corresponding hydrated rutile (001) surface energies of 1.3 to 1.5 J m^{-2}, taken as half the adhesion energy derived from the jump-from-contact force, compare well with the particle-averaged hydrated surface enthalpies of rutile nanoparticles measured by calorimetry (1.9 J m^{-2}) (*15*, *27*).

For jump-to-contact, the measured distance at which the attractive force exceeds the cantilever elastic force is 12 to 20 nm for a nanocrystal tip with a radius of 25 nm. In vacuum at these separations and conditions, the interactions between rutile nanocrystals that conceptually could be relevant are long-range Coulomb and vdW forces (*28*). For jump-from-contact, the similarity in the angular variation and relative magnitude of the measured rupture forces for all background pressures implies that the underlying forces are the same in all cases. Therefore, even at the higher water pressures used here, the relevant forces are expected to be Coulombic and vdW. The former have been rationalized as more dominant in the context of face-specific oriented attachment energies in solution on the basis of classical molecular dynamics simulations (*29*). However, the present experiments were designed to isolate the vdW contribution and so were performed in vacuum on surfaces that should not charge under the electron beam because they are chemically stable, atomically flat, and transect the most electrically conductive direction in rutile (*15*). The jump-from-contact force was reproducible from tip to tip, independent of dwell time under applied load (i.e., point 3 in Fig. 2), and fully reversible with cycling the background water pressure. The applied load was about one-tenth of that needed to displace the anticipated water layer "spacer" trapped between the hydroxylated surfaces (*15*), which means that the surfaces have minimal chance for direct Ti-O(H)-Ti bond formation across the interface. Other short-range interactions that may influence the jump-from-contact force include electrostatic interactions due to the lateral

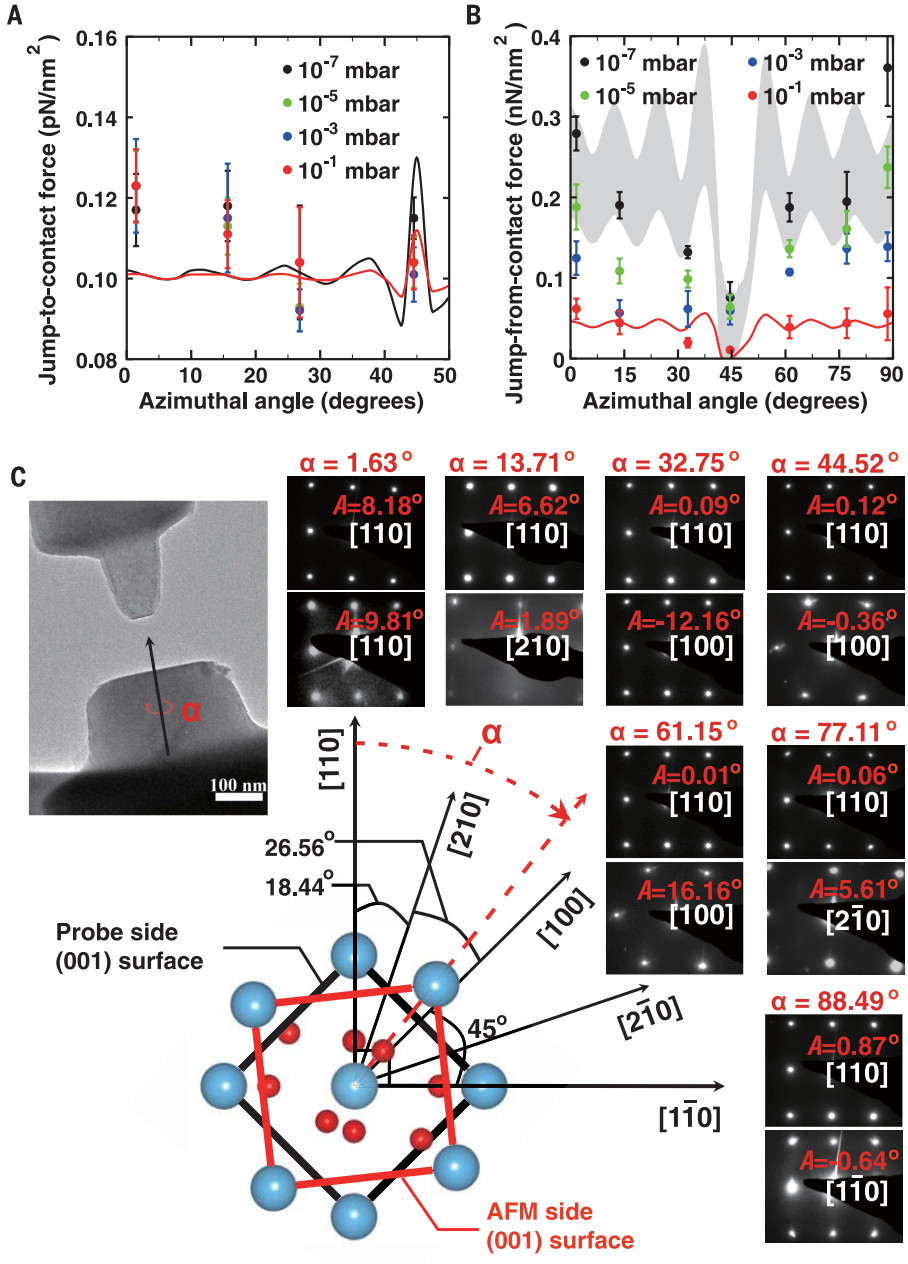

Fig. 3. Dependence of jump-to-contact and jump-from-contact forces on water vapor pressure and azimuthal orientation. (**A**) vdW forces calculated using Lifshitz theory for rutile (001) crystals interacting across vacuum (~10^{-7} mbar) and a thin isotropic water layer (~10^{-1} mbar) are shown with black and red lines, respectively. (**B**) Calculated vdW forces across vacuum at 0.4- to 0.5-nm separation (gray region) and with an intervening isotropic water film at 0.4-nm separation (red line) are shown for comparison to the measured jump-from-contact forces. The TEM image and the crystal model schematic (**C**) (blue spheres represent titanium atoms and red spheres represent oxygen atoms) illustrate the azimuthal orientation α. *A* is the rotation angle of the TEM stage to the low-index zone axis of the crystals (*15*).

variation of electrostatic potential above various atomic sites, and hydrogen bonding interactions due to the formation of water bridges between rutile surfaces. However, the maximum strength of these interactions is more than an order of magnitude smaller than the measured jump-from-contact force (*15*). This leaves the vdW dispersion force as the principal source of interparticle attraction.

To confirm that vdW forces can account for those measured, we calculated the strength of the vdW dispersion interaction as a function of distance and relative orientation within the (001) plane (*15*). The attractive vdW force arises from correlations between fluctuating induced dipole moments in two approaching solids. The theory describing this interaction is well established in Lifshitz theory inclusive of retardation effects (*12*, *15*, *30*–*32*). For dielectrically anisotropic solids like rutile, the theory can be used to calculate direction-specific Hamaker coefficients on the basis of experimental spectroscopic data covering a wide frequency range. We computed these coefficients for rutile (figs. S3 and S4) by combining the measured response from the infrared range (*18*) to the ultraviolet (tables S1 and S2) (*33*) on the basis of anharmonic quantum theory for multiple phonon mode crystals (*15*, *18*–*20*). Calculated static dielectric constants in the *c* direction (154.9) and the average in the *a* plane (84.7) are in good agreement with measurements (160.9 ± 7.0 and 85.5 ± 3.1, respectively) (*18*). We introduced our calculated dielectric response for rutile into Lifshitz theory, including retardation, to predict the strength of the dispersion interaction across the relevant separation range and azimuthal alignment (*15*, *30*).

Calculated and measured force magnitudes are in overall good agreement (Fig. 3, A and B). At a separation of 12 nm, the magnitude of the calculated long-range force is around 0.1 pN nm^{-2} and is predicted to be independent of azimuthal angle or surface water layers, in excellent agreement with the experimental observations (Fig. 3A). This confirms that vdW forces dominate the jump-to-contact interactions. At short range in attractive contact (Fig. 3B), actual separation distances are more uncertain, even in high-resolution imaging mode (*15*), so a distance range of 0.4 to 0.5 nm was used for consistency with the surface roughness observed by TEM and reverse-imaging AFM (fig. S2). Here, theory predicts forces for the vacuum condition in the range of 0.2 to 0.3 nN nm^{-2}, with a minimum below 0.1 nN nm^{-2} at maximum misalignment, consistent with the magnitude and angular dependence of the measured jump-from-contact force. Theory also predicts fine structure in the angular dependence of the force arising from the interplay of angular-dependent and -independent contributions to the Hamaker coefficient. Parsegian *et al.* (*12*) showed that, for dielectrically anisotropic planes, the angular-dependent contribution to the Hamaker coefficient is small compared to the angular-independent contribution when the planes are aligned. Thus, near alignment, one can expect low sensitivity to mutual orientation between the planes. By contrast, at around 45° the angular-dependent part of Hamaker coefficient becomes comparable to the angular-independent one, resulting in a higher sensitivity of the normal vdW force to mutual orientation. These conclusions are consistent with our calculations for rutile (001) surfaces.

At 10^{-1} mbar, the anticipated intervening hydration layer is predicted to diminish the strength of the attraction by dielectric screening of the vdW dispersion. In our experiments, the variation in water pressure between 10^{-7} and 10^{-1} mbar is expected to steadily increase the density of a hydration layer on hydroxylated rutile (001), ultimately stabilizing a water monolayer on each surface at the highest pressure but avoiding condensation of a liquid water thin film (*15*, *21*, *26*). Although the distribution of water across the

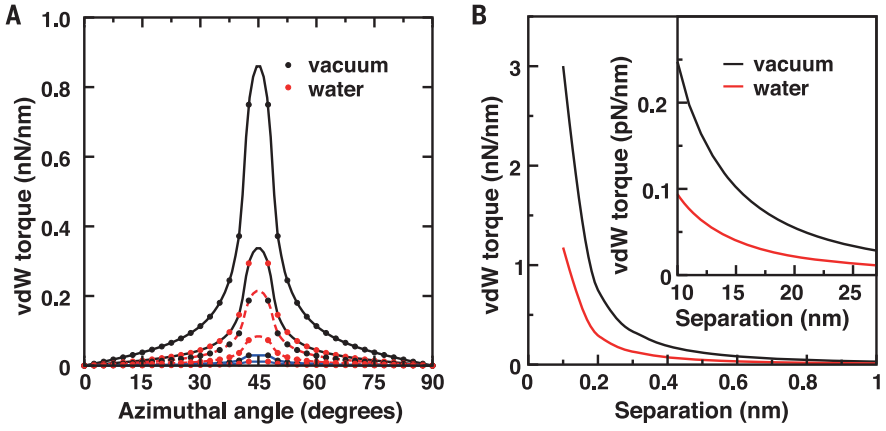

Fig. 4. vdW torque calculated using Lifshitz theory for rutile(001)-rutile(001) at various azimuthal angles and separation distances. (**A**) Angular dependence of the vdW torque at separations of 0.2 nm (black lines), 0.4 nm (red lines), and 1.0 nm (blue lines) across vacuum (black dots) and water (red dots). (**B**) Distance dependence of the vdW torque at an azimuthal angle of 42.5°; the inset features the large-separation region. Torque (nN nm) was computed per unit interfacial area (nm^2), yielding nN nm^{-1}.

surfaces at different water background pressures is not known, the dielectric screening of the vdW interactions by these layers has to be weaker than that from bulk water as the intervening medium (*15*). Assuming that one to two intervening layers of water will be present during attractive contact (*15*), theory again predicts forces in excellent agreement with observations, including a diminished but persistent dependence on azimuthal angle (Fig. 3B). The lack of resolution of the theoretically predicted fine-scale features with azimuthal orientation suggests a role for secondary contributions that limit experimental sensitivity, such as tip edge–substrate interactions, imperfections in surface structure, or interparticle hydrogen bonding (*34*).

The dielectric anisotropy in the *a* plane translates into a vdW torque, which has the same 90° periodicity as the observed jump-from-contact force (Fig. 4A). The calculated vdW torque is the strongest at 45° azimuthal orientation. The angular dependence of vdW forces decreases rapidly with increasing distance between the interacting crystals, and the torque becomes insignificant (smaller than 0.3 pN nm^{-1}) at separations larger than 10 nm (Fig. 4B), consistent with the observed absence of an angular dependence of jump-to-contact forces measured at separations of ≥12 nm (Fig. 3A). The effect of a sparse water layer coating each of the rutile (001) surfaces on the vdW force is also predicted to be small at these large separations, as even the difference between the vdW torque across vacuum and across bulk water is less than 0.1 pN nm^{-1}. The corresponding variations in the vdW forces will then be smaller than 0.1 pN, which explains the invariance of the measured jump-to-contact forces with respect to water background pressure.

These findings demonstrate that in dielectrically anisotropic nanocrystals at close separations, vdW interactions can create substantial torque, even with intervening water layers. More generally, the findings provide a starting point for quantification and understanding of a range of multiscale phenomena that are based on forces sensitive to lattice coalignment. For example, they provide a rational explanation for several important observations concerning the process of crystal growth by oriented attachment. In situ TEM studies of ferrihydrite nanoparticle encounters show that freely diffusing particles pause at separations of about 1 to 2 nm before either rotating to a sufficiently coaligned state and jumping into adhesive contact or succumbing to Brownian motion and diffusing apart (*9*, *35*). Our study shows that vdW forces conceptually can contribute interparticle torque that rotates particles into alignment while solvent separated, increasing the attachment probability of nearly aligned particles, and helps explain why particle encounters far from alignment have a higher rejection rate. Likewise, cryogenic TEM observations of goethite nanoparticle suspensions show that they can spontaneously aggregate and adjust their mutual orientation to form high–aspect ratio rod-shaped "mesocrystals" composed of primary units in crystallographic registry but separated by nanometer-scale solvent layers (*36*). The findings may also help explain self-organization of particles in solution that underlies Schiller layer formation, or the differences in interlayer hydration and swelling behavior in clay minerals relating to layer-stacking polytypism.

REFERENCES AND NOTES

1. R. L. Penn, J. F. Banfield, *Science* **281**, 969–971 (1998).
2. J. J. De Yoreo *et al.*, *Science* **349**, aaa6760 (2015).
3. D. Farrell, C. L. Dennis, J. Lim, S. A. Majetich, *J. Colloid Interface Sci.* **331**, 394–400 (2009).
4. P. M. McGuiggan, J. N. Israelachvili, *J. Mater. Res.* **5**, 2232–2243 (1990).
5. M. Ruths, J. N. Israelachvili, in *Nanotribology and Nanomechanics: An Introduction*, B. Bhushan, Ed. (Springer, Berlin Heidelberg, ed. 2, 2008), pp. 417–515.
6. M. Hirano, K. Shinjo, R. Kaneko, Y. Murata, *Phys. Rev. Lett.* **67**, 2642–2645 (1991).
7. G. S. Rohrer, *J. Mater. Sci.* **46**, 5881–5895 (2011).
8. J. F. Banfield, S. A. Welch, H. Zhang, T. T. Ebert, R. L. Penn, *Science* **289**, 751–754 (2000).
9. D. Li *et al.*, *Science* **336**, 1014–1018 (2012).
10. H.-G. Liao, L. Cui, S. Whitelam, H. Zheng, *Science* **336**, 1011–1014 (2012).
11. H. Zhang, J. F. Banfield, *CrystEngComm* **16**, 1568–1578 (2014).
12. J. C. Hopkins, R. Podgornik, W.-Y. Ching, R. H. French, V. A. Parsegian, *J. Phys. Chem. C* **119**, 19083–19094 (2015).
13. M. L. Sushko, K. M. Rosso, *Nanoscale* **8**, 19714–19725 (2016).
14. E. Finot, E. Lesniewska, J.-C. Mutin, J.-P. Goudonnet, *Langmuir* **16**, 4237–4244 (2000).
15. See supplementary materials.
16. I. Larson, C. J. Drummond, D. Y. Chan, F. Grieser, *J. Am. Chem. Soc.* **115**, 11885–11890 (1993).
17. D. Erts *et al.*, *Appl. Surf. Sci.* **188**, 460–466 (2002).
18. S. Schöche, T. Hofmann, R. Korlacki, T. E. Tiwald, M. Schubert, *J. Appl. Phys.* **113**, 164102 (2013).
19. F. Gervais, B. Piriou, *Phys. Rev. B* **10**, 1642–1654 (1974).
20. F. Gervais, B. Piriou, *C Solid State* **7**, 2374–2386 (1974).
21. P. B. Smith, S. L. Bernasek, *Surf. Sci.* **188**, 241–254 (1987).
22. G. Ketteler *et al.*, *J. Phys. Chem. C* **111**, 8278–8282 (2007).
23. C. L. Pang, R. Lindsay, G. Thornton, *Chem. Rev.* **113**, 3887–3948 (2013).
24. U. Diebold, *Surf. Sci. Rep.* **48**, 53–229 (2003).
25. R. E. Day, G. D. Parfitt, J. Peacock, *Discuss. Faraday Soc.* **52**, 215–225 (1971).
26. P. T. Dawson, *J. Phys. Chem.* **71**, 838–844 (1967).
27. A. A. Levchenko, G. Li, J. Boerio-Goates, B. F. Woodfield, A. Navrotsky, *Chem. Mater.* **18**, 6324–6332 (2006).
28. W. Lv *et al.*, *Nanoscale* **6**, 2531–2547 (2014).
29. H. Zhang, J. F. Banfield, *J. Phys. Chem. Lett.* **3**, 2882–2886 (2012).
30. V. A. Parsegian, *Van der Waals Forces: A Handbook for Biologists, Chemists, Engineers, and Physicists* (Cambridge Univ. Press, New York, 2006).
31. V. A. Parsegian, G. H. Weiss, *J. Adhes.* **3**, 259–267 (1972).
32. Y. S. Barash, *Radiophys. Quantum Electron.* **16**, 945–949 (1973).
33. L. Bergström, *Adv. Colloid Interface Sci.* **70**, 125–169 (1997).
34. M. Raju, A. C. van Duin, K. A. Fichthorn, *Nano Lett.* **14**, 1836–1842 (2014).
35. M. H. Nielsen *et al.*, *Microsc. Microanal.* **20**, 425–436 (2014).
36. V. M. Yuwono, N. D. Burrows, J. A. Soltis, R. L. Penn, *J. Am. Chem. Soc.* **132**, 2163–2165 (2010).

ACKNOWLEDGMENTS

This material is primarily based upon work supported by the U.S. Department of Energy, Office of Science, Office of Basic Energy Sciences, Chemical Sciences, Geosciences, and Biosciences Division under the Geosciences program at Pacific Northwest National Laboratory (PNNL). The development of nanocrystal tip fabrication methods was supported by the Materials Synthesis and Simulations across Scales (MS^3) Initiative, which is a Laboratory Directed Research and Development (LDRD) Program at PNNL. C.W. thanks LDRD seed support for the development of the in situ TEM method. S.X.M. acknowledges support from the National Science Foundation (NSF, CMMI 1536811) through the University of Pittsburgh. The research was performed at Environmental Molecular Sciences Laboratory, a DOE Office of Science User Facility sponsored by the Office of Biological and Environmental Research and located at PNNL. The authors thank M. A. Henderson for helpful discussions.

SUPPLEMENTARY MATERIALS

www.sciencemag.org/content/356/6336/434/suppl/DC1
Materials and Methods
Supplementary Text
Figs. S1 to S4
Tables S1 and S2
Movies S1 to S3
References (*37*–*54*)

1 August 2016; accepted 4 April 2017
10.1126/science.aah6902

Direction-specific van der Waals attraction between rutile TiO_2 nanocrystals

Xin Zhang, Yang He, Maria L. Sushko, Jia Liu, Langli Luo, James J. De Yoreo, Scott X. Mao, Chongmin Wang and Kevin M. Rosso

Science **356** (6336), 434-437.
DOI: 10.1126/science.aah6902

When forces depend on orientation

In oriented attachment, small nuclei or crystals come together to make a larger crystal, but only when complementary facets approach each other. Does this mean that there is an orientational dependence of the force between two nanocrystals? Zhang *et al.* report a delicate method to measure the van der Waals attraction between rutile TiO_2 nanocrystals. They imaged the contact point in situ with environmental transmission electron microscopy, which allowed the interparticle distances to be measured accurately. This elucidated the relationship between the nanocrystals' orientations, surface hydrations, and interactions. The results suggest that there is enough force to generate a torque between the crystals to ensure a complementary interaction.

Science, this issue p. 434